JES Focus Issue on Redox Flow Batteries—Reversible Fuel Cells

The Cell-in-Series Method: A Technique for Accelerated Electrode Degradation in Redox Flow Batteries

Alan M. Pezeshki,[a,b,c,*] Robert L. Sacci,[c] Gabriel M. Veith,[c] Thomas A. Zawodzinski,[a,c,] and Matthew M. Mench[d,e,***,z]**

[a]*Department of Chemical and Biomolecular Engineering, University of Tennessee, Knoxville, Tennessee 37996, USA*
[b]*Bredesen Center for Interdisciplinary Research and Graduate Education, University of Tennessee, Knoxville, Tennessee 37996, USA*
[c]*Materials Science and Technology Division, Oak Ridge National Laboratory, Oak Ridge, Tennessee 37831, USA*
[d]*Department of Mechanical, Aerospace, and Biomedical Engineering, University of Tennessee, Knoxville, Tennessee 37996, USA*
[e]*Energy and Transportation Science Division, Oak Ridge National Laboratory, Oak Ridge, Tennessee 37831, USA*

We demonstrate a novel method to accelerate electrode degradation in redox flow batteries and apply this method to the all-vanadium chemistry. Electrode performance degradation occurred seven times faster than in a typical cycling experiment, enabling rapid evaluation of materials. This method also enables the steady-state study of electrodes. In this manner, it is possible to delineate whether specific operating conditions induce performance degradation; we found that both aggressively charging and discharging result in performance loss. Post-mortem x-ray photoelectron spectroscopy of the degraded electrodes was used to resolve the effects of state of charge (SoC) and current on the electrode surface chemistry. For the electrode material tested in this work, we found evidence that a loss of oxygen content on the negative electrode cannot explain decreased cell performance. Furthermore, the effects of decreased electrode and membrane performance on capacity fade in a typical cycling battery were decoupled from crossover; electrode and membrane performance decay were responsible for a 22% fade in capacity, while crossover caused a 12% fade.
 [DOI: 10.1149/2.0251601jes]

Manuscript submitted August 12, 2015; revised manuscript received October 29, 2015. Published November 21, 2015. This was Paper 371 presented at the Orlando, Florida, Meeting of the Society, May 11–15, 2014. *This paper is part of the JES Focus Issue on Redox Flow Batteries–Reversible Fuel Cells.*

The vanadium redox flow battery (VRFB) is a potential grid-scale energy storage technology that has attracted significant research interest.[1–5] The cell architecture, electrodes, and membranes have been considerably optimized, resulting in increased efficiency and power density of VRFBs.[3,5–10] Other research has focused on improving energy density by enhancing vanadium solubility through the use of additives in the electrolyte solution; these compounds may also enhance electrode activity.[11–13] As these improvements continue, the long-term durability of VRFBs becomes an issue with strong implications for commercial viability. Therefore, methods to study component durability are of growing interest.

Unlike traditional secondary batteries, VRFBs do not suffer from appreciable unrecoverable capacity fade. They promise to have long lifetimes due to the ability to rebalance the electrolyte,[14–16] which negates capacity fade and may allow them to last for thousands of cycles and for several years. While the vanadium electrolyte is stable,[17] the durability of some components in the VRFB has not been studied in detail. Changes in the electrode can result in increased activation/charge transfer resistance and decreased mass transport; changes in the membrane may result in increased ohmic resistance in the cell. These phenomena contribute to a decrease in the capacity that can be accessed at high currents as well as to reduced energy efficiency. Herein, we present a methodology and initial findings for studying performance degradation in VRFBs. The energy efficiency loss in a typical VRFB cycling experiment is deconvoluted into contributions from decreased electrode performance and increased ohmic resistance within the membrane. The capacity fade mechanism, often attributed to crossover alone, is examined and the relative contributions of crossover and increased cell overpotential are discussed. Electrode changes are the focus of this study; therefore, changes in the membrane related to long-term durability are not discussed in great detail in this work.

A link between electrode aging and oxygen content has been established in the literature;[18,19] however, it remains unclear as to what operating conditions cause the oxidation, and to what degree electrode performance, and ultimately the energy efficiency, is affected. Trogadas and coworkers analyzed cycled carbon felts and found microstructural defects, a large increase in oxygen content, and a decrease in surface area after 60 h of cycling.[18] Mohammadi and Skyllas-Kazacos examined graphite felts after overcharge and saw differing degrees of oxidation based on the specific type of felt used.[19] Rudolph and coworkers investigated capacity fade and losses in energy efficiency in VRFBs and suggested that passivation related to the loss of hydroxyl groups on the negative electrode surface increased the internal resistance of the battery.[14,20] A few studies discuss corrosion of graphite materials in VRFBs,[21–23] though these materials are typically used as the flow field and not the primary surface on which the electrochemistry is occurring.

It is well known that the electrode surface chemistry and surface area determine the activation overpotential[24,25] in the electrode. Several reports have concluded that oxygen and nitrogen functionalization of carbon materials can be effective means of altering surface chemistry to promote the vanadium redox reaction kinetics, reducing activation overpotential and improving performance.[26–38] Di Blasi et al. suggested that there is an optimal amount of oxygen for a VRFB electrode, beyond which electrode performance decreases.[39] As previous studies show a link between aging and oxidation of the surface,[18,19] the question of how aging-induced oxidation affects the chemistry of an already-oxidized surface, and ultimately the electrode performance, is of interest.

Typical cycling experiments involve varying the state of charge (SoC) and alternating the direction of current, making it difficult to determine when electrode degradation occurs. To resolve the effects of SoC and charge/discharge condition on the surface chemistry of the

*Electrochemical Society Student Member.
**Electrochemical Society Fellow.
***Electrochemical Society Active Member.
[z]E-mail: mmench@utk.edu

electrode, we developed a novel cell-in-series (CIS) technique that maintains a constant SoC at a particular charge/discharge condition for indefinite periods of time. The CIS technique was used at high and low voltages to artificially stress the electrodes, which resulted in relatively rapid decreases in performance relative to a cell that underwent typical cycling. This indicates that the CIS is a useful tool for accelerated VRFB testing. The technique is broadly applicable to flow batteries involving two liquid-phase redox reactions; it cannot be applied to hybrid flow batteries in which one electrode undergoes electroplating or electrodissolution because a steady state cannot be maintained.

Overall, this work presents the CIS technique as a tool to age electrodes at different sets of specified steady-state conditions. The use of x-ray photoelectron spectroscopy (XPS) demonstrates how an analytical method can be used to identify specific changes in the physicochemical properties of the electrode due to differing operating conditions within the battery. The electrical double layer capacitance of the electrodes was also measured and used as a proxy for the electrochemically active surface area. The surface oxygen content (from XPS) and surface area were assessed as two possible causes of the observed electrode performance degradation.

Experimental

In this work, electrodes are degraded at typical conditions in a cycling experiment, high and low SoC under charge and discharge conditions via the CIS method, and by chemical means through soaking in electrolyte solution. Polarization curves are used to characterize electrochemical performance and XPS is used to quantify oxygen content of selected electrodes. Capacitance measurements are used to estimate the electrochemically active surface area.

Cell architecture.— Single-cell flow batteries using the no-gap architecture[6] with a single-channel serpentine flow field design were used. One layer of SGL 10AA carbon paper (SGL Group) compressed to 70% of its original thickness was used as the electrode in both sides of the cell. Geometric active areas of 5 and 25 cm^2 were used. All 5 cm^2 electrodes were heat treated in 42% oxygen / 58% nitrogen (Airgas) at 400°C for 30 h prior to use;[10] 25 cm^2 electrodes were used as received. Nafion 117 (DuPont) was used as the membrane in all cells. Cell temperatures were controlled at 30°C with an Arbin FBTS 2000. Electrochemical measurement and control for cycling and CIS testing were performed with an Arbin FBTS 2000. Electrochemical measurement and control for cyclic voltammetry and electrochemical impedance spectroscopy (EIS) used to determine the capacitance were carried out with a Bio-Logic Instruments VSP potentiostat. Polarization curves were obtained with the Bio-Logic VSP potentiostat coupled to a 20 A booster.

Electrolyte solutions.— Solutions of 1.7 M vanadium ions in 5 M total sulfate were prepared from vanadium sulfate oxide hydrate (Alfa Aesar, 99.9%) and sulfuric acid (Alfa Aesar, ACS grade). Initial charging was performed with a 2:1 catholyte:anolyte volume ratio in a 25 cm^2 cell at 1.8 V until a cutoff current of 10 mA/cm^2 was reached. One half of the catholyte solution was then discarded to obtain a 1:1 volume ratio of ca. 100% SoC catholyte and anolyte solutions. Electrolyte tanks were purged with nitrogen (Airgas, UHP) to prevent oxidation of the vanadium species. Separate sets of solution were used for soaking, CIS, cycling, and polarization curve experiments as described below.

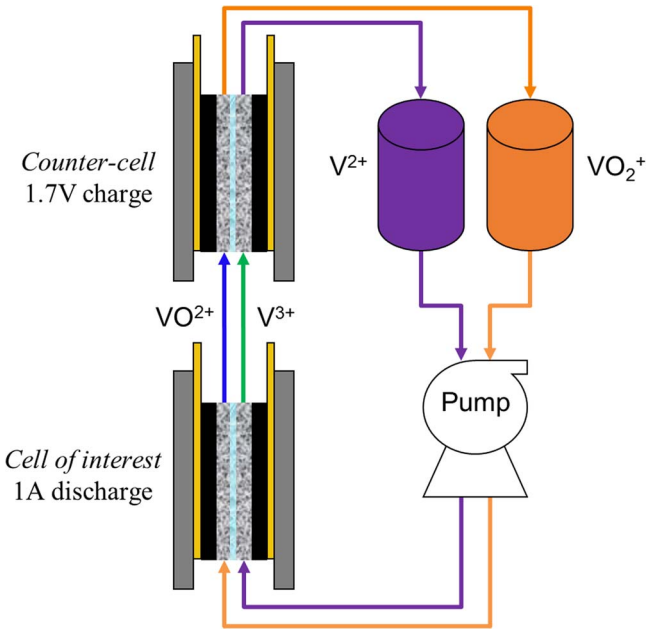

Figure 1. Schematic of CIS set-up with discharge occurring in cell of interest and recharge occurring in counter-cell.

Cycling.— A single-cell battery with 5 cm^2 geometric active area was used to carry out cycling at a current density of 200 mA/cm^2. Cutoff voltages of 1.0 V and 1.65 V for discharge and charge, respectively, were used. 50 mL of catholyte and anolyte were circulated at 90 mL/min.

Cell-in-series.— In this work, the CIS method is introduced as a way to maintain constant conditions for flow battery testing. Two single-cell batteries were used, as shown in Fig. 1; each battery is controlled by an independent channel on the potentiostat. The first cell, which will be described as the "cell of interest" in the remainder of this work, consists of a 5 cm^2 geometric active area with heat-treated carbon paper electrodes; the second cell, described as the "counter-cell," consists of a 25 cm^2 geometric active area with untreated carbon paper electrodes. 50 mL of catholyte and anolyte were recirculated for the duration of testing with a dual channel peristaltic pump (Cole Parmer) at 20 mL/min through the cell of interest and then through the counter-cell before returning to the electrolyte reservoirs. For cases in which the cell of interest was galvanostatically controlled, the counter-cell was potentiostatically controlled; when the cell of interest was potentiostatically controlled, the counter-cell was galvanostatically controlled. A summary of these control schemes is listed in Table I.

Table I. Summary of electrochemical data for cell-in-series experiments. Positive currents denote charging; negative currents denote discharging.

Experiment	Cell of interest (5 cm^2) control mode	Counter-cell (25 cm^2) control mode	SoC	Cell of interest average voltage [V]	Coulombic efficiency
A	+100 mA	1.0 V	Low	1.289	91.6%
B	+1000 mA	1.0 V	Low	1.501	98.3%
C	−100 mA	1.7 V	High	1.530	90.2%
D	−1000 mA	1.7 V	High	1.206	97.4%
E	0.6 V	+100 mA	Low	0.600	91.4%
F	1.8 V	−100 mA	High	1.800	89.5%

Soaks.— The 100% SoC solutions (V^{2+} and VO_2^+) were obtained as described above. The ~0% SoC solutions (V^{3+} and VO^{2+}) were obtained by discharging 100% SoC solutions until a cutoff potential of 0.2 V was reached; an open-circuit voltage (OCV) of ca. 1.2 V was observed. Strips of the heat-treated electrode material were immersed in vials of the prepared solutions and purged with nitrogen and sealed. Soaks were carried out for 3 d and 6 d at room temperature.

Electrochemical measurements.—Polarization curves.— Polarization curves were obtained with separate sets of electrolyte solutions with volumes of ca. 400 mL. In the first set of experiments, the polarization curves were taken with cells that were previously cycled or run in the CIS set-up; in these cases, the cell was drained of electrolyte solution and tanks were replaced with the polarization curve solution tanks. In the second set of experiments, cells were built with electrodes that had been previously soaked in electrolyte solution but not electrochemically cycled. In these cases, electrodes soaked in catholyte were used as the positive electrode and electrodes soaked in anolyte were used as the negative electrode. During all polarization curve measurements, the counter-cell was removed from the fluid circuit (i.e., electrolyte flowed only through the cell of interest).

For all polarization curves, a relatively high flow rate of 90 mL/min was used to minimize concentration polarization. The catholyte and anolyte were ca. 50% SoC, obtained by coulometric discharge of the 100% SoC solution. Because large volumes of electrolyte were used and the current passed was low, and charge and discharge nearly balanced out, changes in SoC during polarization curves were minimal. Polarization curves were obtained with potential steps beginning at OCV and then in increments of ±20 mV. The current value was taken as the average over the last 15 s for each potential step, after a steady-state current had been reached (less than 5 s was required to reach steady-state).

Electrochemical impedance spectra were obtained during the potentiostatic control steps to measure the high-frequency resistance (HFR), which was taken as the intercept of the Nyquist spectrum with the real axis. The areal specific resistance (ASR) was obtained by multiplying the HFR by the cell geometric area. The ohmic drop was calculated multiplying ASR by the current density; this value was subtracted from the applied cell voltage for *iR*-correction.

Capacitance.—The capacitance of the electrode materials was obtained in an ex situ three electrode cell. Measurements were obtained after samples were cleaned (described in the XPS section below). A single layer of carbon paper was clamped between graphite clips and immersed in 0.5 M sulfuric acid and used as the working electrode in conjunction with a mercury sulfate reference electrode (Pine Instruments) and platinum mesh counter electrode. The carbon paper was preconditioned with 10 cycles of cyclic voltammetry carried out between –0.5 and 0.5 V at a scan rate of 50 mV/s, followed by EIS performed at constant applied voltages of –0.5 to 0.5 V in 0.1 V increments.

X-ray photoelectron spectroscopy.— Used or electrolyte-soaked electrode materials from three day CIS operation were triple rinsed in DI water and dried at 75°C in air for 2 h prior to XPS analysis. Samples were loaded into an ultra-high vacuum chamber which was maintained at 10^{-8} Torr or less during measurement. Spectra were taken with a PHI 3056 spectrometer with an Al K_α x-ray source (1486.6 eV) at 350 W. Survey scans were taken with 0.5 eV energy steps and a pass energy of 93.9 eV; high resolution scans were taken with 0.05 eV energy steps and a pass energy of 23.5 eV. Spectra were charge-corrected by setting the highest intensity carbon peak to 284.8 eV. The C1s and O1s high resolution scans were processed by subtracting a Shirley-type background and then normalized by the maximum intensity within the same sample.

Results and Discussion

Cycling.— Representative cycling data for a VRFB operated at 200 mA/cm^2 are shown in Fig. 2a. The cell exhibited stable coulombic efficiency while the voltage efficiency (VE) declined slightly from 78% to 75% over the course of the experiment. After 54 cycles (6 d of operation, ~3 h/cycle), the capacity faded to 66% of the first cycle capacity. It has been well established that crossover affects capacity by causing an imbalance in the vanadium concentrations; the side with less vanadium restricts the total capacity of the battery, resulting in capacity fade. The capacity can be restored by rebalancing electrolyte to the initial concentrations of vanadium in each half-cell.[15] The electrolytes were rebalanced after the 54th cycle and the solution was recharged in a separate cell to verify that the vanadium concentrations were restored to the first cycle values. The initial charge capacity of the electrolyte after the rebalance operation was 99% of the initial charge prior to the first cycle, indicating that side reactions were not responsible for significant capacity fade under the cycling conditions used in this experiment.

Charge and discharge profiles for cycles 1, 54 (pre-rebalance), and 55 (post-rebalance), presented in Fig. 2b, show a 50 mV increase in the charging voltage between cycle 1 and cycle 54 in the linear region of the charge curve, while the discharge profiles showed a 55 mV decrease in the same region. Imbalances in the vanadium concentration can explain part of this shift, as concentration imbalances can

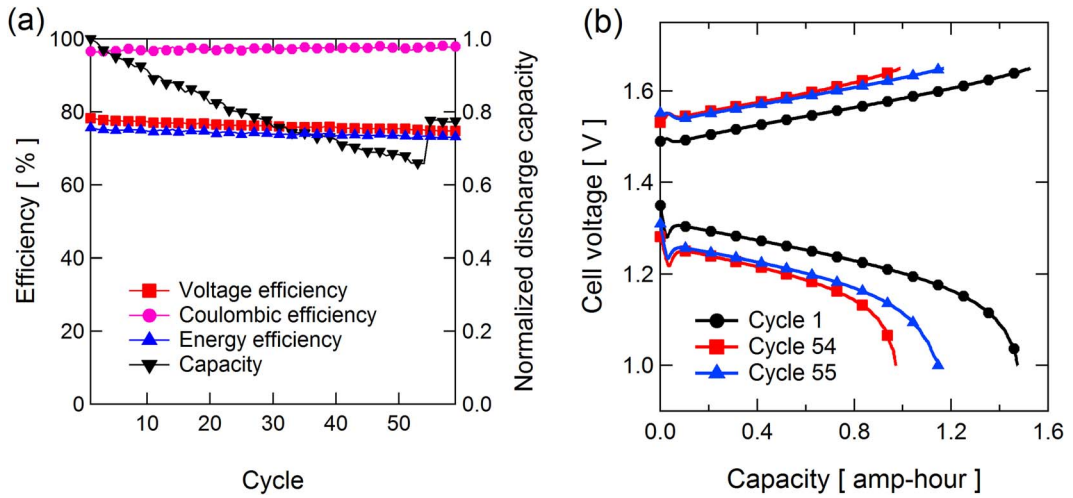

Figure 2. Results for battery cycled at 200 mA/cm^2 with electrolyte solution rebalance between cycles 54 and 55: (a) voltage efficiency, coulombic efficiency, energy efficiency, and discharge capacity and (b) charge and discharge profiles.

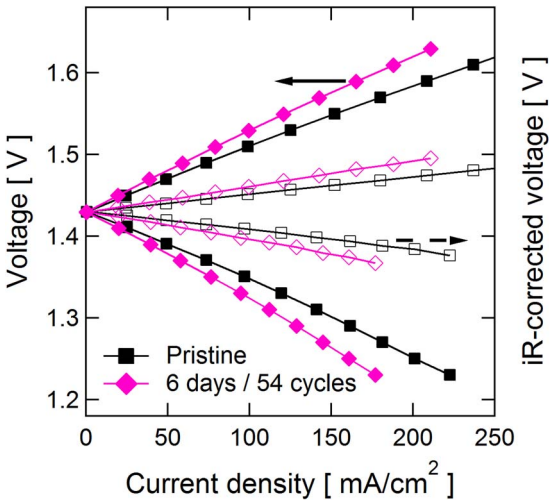

Figure 3. Polarization curves before and after 54 cycles at 200 mA/cm^2. Solid symbols reflect uncorrected data; hollow symbols are *iR*-corrected. Left and right axis scales are identical.

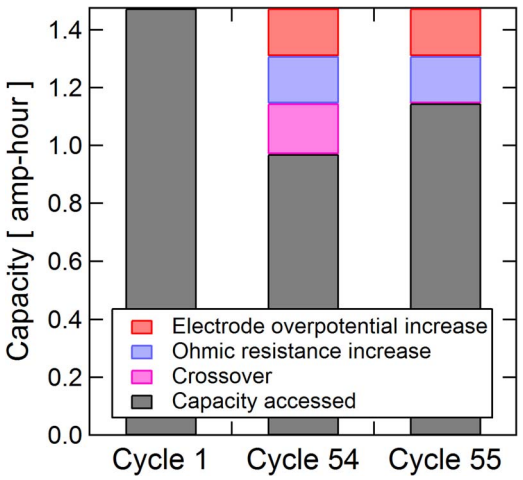

Figure 4. Capacity fade after 54 cycles attributed to crossover, increased membrane resistance, and decreased electrode performance, denoted as the sum of increased transport and kinetic overpotential.

impact the OCV and therefore the charging and discharging profiles. However, even after rebalancing and restoring the initial vanadium concentrations, the cycle 55 charging and discharging profiles were similar to the cycle 54 profiles, with only a 5 mV decrease in the charge profile and a 7 mV increase in the discharge profile. Though vanadium concentrations were restored after cycle 54, the next cycle's capacity was only 78% of the first cycle's capacity, indicating that electrolyte crossover only caused a 12% drop in capacity while another process caused capacity to drop an additional 22%.

The observed 22% decrease in capacity can be explained by an increase in the battery overpotentials over the course of cycling. An increase in the charging overpotential results in reaching the upper voltage limit at a lower SoC, effectively cutting the charge capacity. Likewise, on discharge, a larger overpotential results in reaching the lower voltage limit at a higher SoC, decreasing the discharge capacity. As a result, the OCV after charging is lower and after discharging is higher, which partially explains the changes in the charge and discharge profiles. The remaining portion of the shift is due to the increase in overpotentials, not the equilibrium potential. In this work, polarization curves are utilized to measure the changes in the battery overpotential.

In electrochemical cells, overpotentials are attributed to electrochemical activation (charge transfer), ohmic, and concentration polarizations.[40] Polarization curves were obtained before cycle 1 and after cycle 54 to identify changes in the cell overpotential; use of a separate solution ensured that the results were independent of crossover effects that occur during cycling. The polarization curves shown in Fig. 3 include both the *iR*-corrected and uncorrected data. Because the *iR*-corrected curves remove the ohmic overpotential from the membrane, changes in the *iR*-corrected curves in Fig. 3 are attributed to changes in the kinetic performance of the electrode surface, changes in the mass transport behavior within the cell, or a combination of the two. A 20 mV increase in the sum of the activation and mass transport overpotentials at a current density of 200 mA/cm^2, from 45 mV pre-cycling to 65 mV post-cycle 54, was observed. More work must be done in order to conclusively resolve the activation/kinetic overpotential increase and the mass transport/concentration overpotential increase. An increase in the activation overpotential is indicative of a decrease in the electrode's electroactive surface area, a decrease in the electrode activity, or a combination of the two. A decrease in activity is due to inherent changes in the nature of the electrode surface and in the case of a carbon electrode is related to the structure of the carbon itself as well as the presence of heteroatoms such as oxygen. Few studies discuss changes in the electrode due to usage in an operational VRFB. Regarding properties that might alter electrode kinetics, Trogadas et al. observed a decrease in the active surface area of carbon felt electrodes of 37% after 60 h of cycling due to fiber agglomeration.[18] Rudolph et al. speculated that a loss of oxygen-containing functional groups on the negative electrode resulted in decreased electrode activity.[14,20] Changes in mass transport, if present, are likely attributable to changes in the electrode morphology that impact electrolyte flow. One such change may be related to fiber agglomeration observed in reference 18, which would affect the electrode tortuosity. Another possible mechanism that could cause such changes would be the dislodging of carbon particles from the electrode. These particles could eventually clog portions of the electrode, impeding the bulk transport of vanadium species throughout the electrode. We mention these as two possible mechanisms by which transport can be affected within the electrode; other mechanisms are possible and should be investigated. The VRFB literature to date does not comment on changes in mass transport that may occur during cycling.

The ASR measured during discharge at a current density of 200 mA/cm^2 increased from 0.66 to 0.77 Ω cm^2 after 6 d of cycling; over the same time period, the ASR during charge increased from 0.55 to 0.64 Ω cm^2. Vijayakumar et al. observed that VO^{2+} ions can foul Nafion-based membranes,[41] reducing conductivity and increasing the cell resistance. Translated to the cycling experiment at 200 mA/cm^2, the increase in ASR resulted in 18 mV of additional overpotential during charging and 22 mV during discharging. Therefore, the decline in the cell's cycling performance is caused by an increase in the membrane resistance as well as decreased electrode performance, which must result from worsening kinetic properties, mass transport, or a combination of the two. Both components experienced an approximate 20 mV increase in overpotential, meaning that the cell's overall performance decline is due in equal parts to membrane and electrode performance loss. A summary of the contributions to capacity fade through cycle 54 of cycling is shown in Fig. 4. Given that the previously described polarization curves demonstrate that the increases in overpotential due to the membrane and electrodes are equal in magnitude, the 22% capacity fade due to increased cell overpotential, described above, is ascribed evenly to membrane and electrode contributions.

We briefly note that one might expect a 50 mV increase in the linear region of the charging profile and a 50 mV decrease in the linear region of the discharging profile to result in a much larger drop in VE than the observed 3% (78% to 75%.) However, because voltage cutoffs are used to end the charge and discharge steps (1.65 and 1.0 V, respectively), the average voltage cannot change to the same

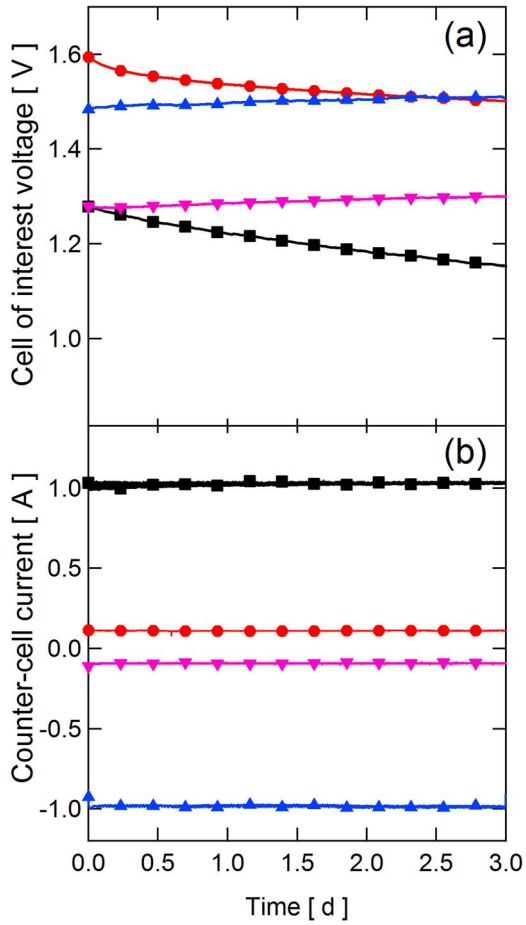

Figure 5. Electrochemical data for experiments A–D, in which the cell of interest was galvanostatically charged: (a) cell of interest voltage and (b) counter-cell current. Symbols refer to experiments as follows: (▼) A, Low SoC +20 mA/cm^2, (▲) B, High SoC +200 mA/cm^2, (●) C, High SoC –20 mA/cm^2, (■) D, High SoC –200 mA/cm^2.

extent that the overpotential does. For example, the cycle 1 average charge voltage was 1.562 V, while the cycle 55 average charge voltage was 1.589 V, an increase of only 27 mV; this is much lower than the overall 50 mV shift observed in the overall charge profile. The use of different voltage cutoffs or state-of-charge cutoffs instead of voltage cutoffs to increase the charge and discharge windows would decrease capacity fade, but result in lower voltage efficiencies over time as the cell overpotential increases.

Cell-in-series.— A summary of the conditions tested and the resulting electrochemical data is shown in Table I. For simplicity, this portion of the discussion focuses on the four conditions (experiments A–D) in which the cell of interest was galvanostatically controlled and the counter-cell was potentiostatically controlled. Potentiostatic control in the counter-cell is desirable, as the large active area ensures a low current density and therefore low overpotentials. In this manner, very high and very low SoC operating conditions can be maintained: holding the counter-cell at 1.7 V yields ca. 95% SoC based on coulombic calculations; a potential hold at 1.0 V results in ca. 5% SoC. Galvanostatic control is chosen in the cell of interest to ensure the desired current is reached. Though steady state currents should lead to steady voltages, the voltage declined for discharging cells (A, B) by over 100 mV and increased by 20 mV for charging cells (C, D), as seen in Fig. 5a. Some portion of the change in the cell voltage can be explained by crossover, as the self-discharge due to crossover decreases the OCV. When the OCV is decreased, the cell voltage with passage of current will also decrease; the changes in concentration due to crossover can also have minor impacts on the concentration and activation overpotentials. Other changes in the cell voltage independent of crossover are attributed to decreasing electrode performance, discussed in the polarization curve section below in more detail, and increasing membrane resistance. The current in the counter-cell in each case was extremely stable over the course of the experiment, shown in Fig. 5b. The steady current indicates that a relatively steady SoC was achieved. It is noted that the charging cell always had a slightly higher current than the discharging cell due to crossover that occurs in both the cell of interest and the counter-cell.

To achieve extreme conditions in experiments E and F, i.e. charging while at high SoC and discharging while at low SoC, potentiostatic control is used in the cell of interest and galvanostatic control is used in the counter-cell. Because the cell overpotentials increase over time, maintaining galvanostatic control in the cell of interest while charging at high SoC would result in very high cell voltages that are unrealistic for VRFB operation due to high rates of undesirable gas evolution reactions and corrosion of the graphite blocks. Therefore, the cell of interest must be controlled potentiostatically. The counter-cell is controlled galvanostatically to ensure that current will also pass in the cell of interest; potentiostatic control in both cells with continued increase in the cell of interest overpotential would eventually result in no current passed.

The coulombic efficiency in Table I is calculated by dividing the average discharge current by the average charge current. Though a detailed discussion of coulombic efficiency is beyond the scope of this paper, it is noted that some information regarding crossover is available from the coulombic efficiencies found with the CIS experiment, as crossover is what drives the coulombic efficiency to be less than 100%. For example, experiments carried out at low current (A, C, E, F) had a coulombic efficiency of 90–92%, while those at high current (B, D) had a coulombic efficiency of 97–98%, implying that crossover occurs at higher rates when the cell operates at lower current densities. These results agree qualitatively with recent literature where the authors also found that increased current density operation results in improved coulombic efficiency.[42] For further insight into the relative rates of migration and diffusion and how these affect the net crossover, and ultimately coulombic efficiency, see reference 42. Experiments at high SoC had more rapid crossover than those at low SoC: at high current, the coulombic efficiency of experiment D (97.4%) was lower than B (98.3%), and at low current, experiments C and F (90.2, 89.5%) had lower coulombic efficiencies than A and E (91.6, 91.4%). These results are logical in that the passage of the charged V^{2+} and VO_2^+ species through the membrane results in more self-discharge, and thus effectively faster crossover, than the passage of the discharged V^{3+} and VO^{2+} species. In summary, the CIS technique could be useful in parametrically studying crossover as a function of operating parameters with relative ease.

CIS/soak polarization curves.— As described above, *iR*-corrected polarization curves in this work are indicative of a combination of activation and mass transport losses. As shown in Figs. 6a and 6b, operation at a fixed voltage, whether at low SoC and discharging (experiment E, 0.6 V hold, −20 mA/cm^2) or at high SoC and charging (experiment F, 1.8 V hold, +20 mA/cm^2) serves to greatly decrease electrode performance. It is noted that the increase in overpotential is observable at low current densities (20 mA/cm^2), which suggests a decrease in kinetic performance. The slope of the polarization curve increases throughout the curve, which may indicate that transport within the cell also declines. More work must be done to determine the chief contributor to electrode performance loss. For both experiments E and F, there was an increase in *iR*-corrected overpotential at a current density of 100 mA/cm^2 from ca. 25 mV before CIS operation to 65 mV and 100 mV after 3 d and 6 d of CIS operation, respectively. Since the increases in overpotential are similar, the detrimental changes in the electrode performance cannot be attributed solely to charging or discharging. In comparison, the overpotential at 100 mA/cm^2 observed in the cycling experiment increased from 25 mV pre-cycling to 35 mV after 6 d of cycling. The increase in

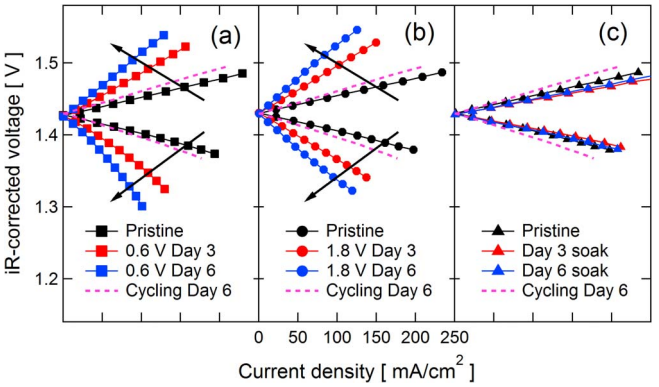

Figure 6. *iR*-corrected polarization curves taken after initial build, 3 d, and 6 d: (a) cell-in-series experiment E: potential hold at 0.6 V and at low SoC, (b) cell-in-series experiment F: potential hold at 1.8 V and at high SoC, and (c) soaked in high SoC solution. Curve for cell cycled for 6 d shown for reference.

overpotential due to CIS operation (75 mV) was thus sevenfold larger than the increase in overpotential due to cycling (10 mV). This indicates that the experimental conditions in E and F likely simulate much longer cycling time, which is logical since cycling experiments reside in the neighborhoods of 0.6 or 1.8 V for very short periods of time. These tests may be a valuable method in evaluating the durability of electrode materials due to the accelerated performance degradation observed.

The effects of high SoC electrolyte on the electrodes, without the presence of any electrochemical effects, is shown to be minimal with respect to performance, as the polarization curves in Fig. 6c indicate that the *iR*-corrected overpotentials actually slightly decrease after 3 d and 6 d of electrolyte exposure. Overall, then, the polarization curves suggest the decline in electrode performance cannot be attributed to the chemical effects of exposure to strong oxidizing (VO_2^+) or reducing agents (V^{2+}). Rather, the loss in performance likely originates from electrochemical processes (the passage of current). Furthermore, soaking electrodes in the electrolyte is not a sufficient method by which electrode durability can be tested, though it is often used in predicting the long-term stability of ion exchange membranes used in VRFBs.[9,43]

Physicochemical characterization.— The electrode surface is the determining factor for the reaction kinetics and thus the activation overpotential. The relevant surface properties include the electrochemically active surface area as well as the surface chemistry, which affects the activity of the surface. As described in the introduction, it has been claimed that the presence of certain oxygen functional groups reduces the activation overpotential for vanadium redox reactions. In the following sections, changes in the surface area and oxygen functional groups as a result of usage in the battery and their potential contributions to performance loss are discussed.

Capacitance.—The double layer capacitance is used as a proxy for the surface area, i.e., it is assumed that the surface area is proportional to the double layer capacitance. It is noted that the presence of oxygen functional groups can affect the capacitance; however, these changes are not expected to affect the capacitance by more than 25%.[44] In order to estimate the capacitance, an equivalent circuit model consisting of a constant phase element in series with a resistor was used to fit the impedance data obtained in the three electrode cell, similar to the analysis performed by Sun et al.[45] The double layer capacitance was estimated at each voltage following Brug et al.:[46] $C_{dl} = (Q_0 R_\Omega^{1-\alpha})^{1/\alpha}$ and is shown in Fig. S1. The cyclic voltammogram in Fig. S2 was taken immediately prior to obtaining impedance data. A sample fit is also shown in Fig. S3.

No clear trend was observed in the capacitance in relation to SoC or operating conditions; i.e., some of the samples exposed to catholyte experienced increased capacitance while others experienced decreased capacitance, and likewise for those exposed to anolyte. In addition, there were no trends relating poor electrochemical performance to changes in capacitance: the electrodes soaked in 100% SoC catholyte experienced a 50% decrease in capacitance relative to the pristine electrode, while the electrodes soaked in 100% SoC anolyte experienced a small increase in capacitance. The cell built with these electrodes as the positive and negative electrodes, respectively, then, had an overall decrease in the surface area. However, the electrode performance was improved, as shown in Fig. 5c. Furthermore, the changes in capacitance are small when compared to the effect of the initial heat treatment, in which the capacitance increases by a factor of 200[10]. Therefore, the data suggest that a change in the surface area cannot explain the majority of the observed increase in electrode polarization.

XPS.—XPS spectra focused on the O1s region are presented for electrodes subjected to the CIS tests or soaked in electrolyte. The C1s region also shows changes, but the changes are less apparent due to the high concentration of C–C species and are therefore are not shown. The O1s peak maximum is typically at or around 533.5 eV, and is attributed to C–O bonds; spectral intensity which appears at 532 eV as a shoulder to the main peak is attributed to C=O bonds. Two versions of the same data are shown: the O1s spectra normalized to the C1s peak shows the relative concentration of oxygen on the carbon surface within each sample; the O1s spectra normalized to the O1s peak shows the peak shape and therefore the relative distribution of C–O to C=O bonds. The oxygen content of the pristine electrode surface was 2.5%; after soaking in sulfuric acid, surface oxygen increased to 5.5%. The acid-soaked electrode is used as the relevant reference point. No observable quantities of sulfur from the sulfuric acid were present in the XPS spectra. A summary of oxygen contents is shown in Table II.

As shown in Fig. 7a, exposure to V^{2+} decreased the oxygen content from 5.5% in the acid-soaked sample to 3.1%; V^{3+} decreased the oxygen content to 5.1%, VO^{2+} showed no effect, and VO_2^+ increased the oxygen content to 9.3%. Indicated in Fig. 7b, there is a clear difference in the C–O/C=O surface chemistry after exposure to the electrolytes, the catholyte inducing more C=O bonding relative to C–O than the anolyte, evident in the increased spectral intensity at 532 eV.

Shown in Fig. 7c, SoC was the dominant force in affecting the oxygen content in the positive electrode, as the electrode always exhibited a higher oxygen content at high SoC – 6.9% or greater, compared to 6.4% or less for low SoC – independent of whether the cell was charging or discharging and independent of the magnitude of the applied current. The direction of current (i.e., charging vs discharging) was not important at the low current density: at both low and high SoC, the + and −20 mA/cm^2 spectra are nearly overlaid. The effect of the magnitude of the applied current was most apparent in the bonding in Fig. 7d: the high current density experiments, independent of high or low SoC, enhanced the C=O bonding relative to the C–O bonding. The effect of SoC is secondary, though at the lower current density, the high SoC induced more C=O bonding, similar to what was observed in the soaking experiments described previously. That the C=O bonding was enhanced by both high current densities and electrolyte soaking is somewhat puzzling, as one might expect the electrolyte soaks and the low current density experiments to be similar because a low current density is closer to the equilibrium or zero current density experienced during electrolyte soaking.

Apparent from the spectra for the negative electrodes, shown in Fig. 7e, is that the oxygen content on the negative electrode was generally similar to or less than that observed with the sulfuric acid soak, opposite of what was observed on the positive side. No clear trends appear that link oxygen content to SoC, magnitude of current, or direction of current. However, the C=O bonding, shown in Fig. 7f, exhibited a slight decrease relative to the C–O bonding in all cases, and furthermore, a high SoC typically reduced the C=O bonding more than a low SoC.

Table II. Atomic composition of electrode surface for cell-in-series and electrolyte soak experiments as determined by XPS analysis, sorted from maximum to minimum oxygen content.

Experiment	Oxygen content [atomic %]	Carbon content [atomic %]	Electrode Polarity	SoC	Current density [mA/cm^2]
V(V) soak	9.3	90.7	+	High	N/A
F	8.3	91.7	+	High	+20
C	8.0	92.0	+	High	−20
D	6.9	93.1	+	High	−200
B	6.4	93.6	+	Low	+200
A	5.8	94.2	+	Low	+20
B	5.7	94.3	−	Low	+200
E	5.7	94.3	+	Low	−20
D	5.5	94.5	−	High	−200
V(IV) soak	5.5	94.5	+	Low	N/A
acid soak	5.5	94.5	N/A	N/A	N/A
A	5.1	94.9	−	Low	+20
V(III) soak	5.1	94.9	−	Low	N/A
F	4.4	95.6	−	High	+20
E	3.5	96.5	−	Low	−20
V(II) soak	3.1	96.9	−	High	N/A
pristine	2.5	97.5	N/A	N/A	N/A

The overall XPS results, qualitatively shown in Fig. 8, suggest that the electrode surface chemistry is indeed affected by operating conditions. Relative to soaking in acid, an electrode in the positive half-cell of the battery undergoes significant oxidation when at a high SoC under a variety of operating conditions, while the positive electrode at low SoC and the negative electrode at both low and high SoC both show little evidence of oxidation under similar applied currents. The general trend of oxidation of the positive electrode surface agrees with other literature, though the amounts vary significantly. With the carbon papers used in this work, the highest post-mortem oxygen content observed was 9.3%, much lower than the 40% observed after 65 hours of cycling[18] or 18–30% observed after 50 min of overcharge.[19] While more investigation is needed, these results are an indication

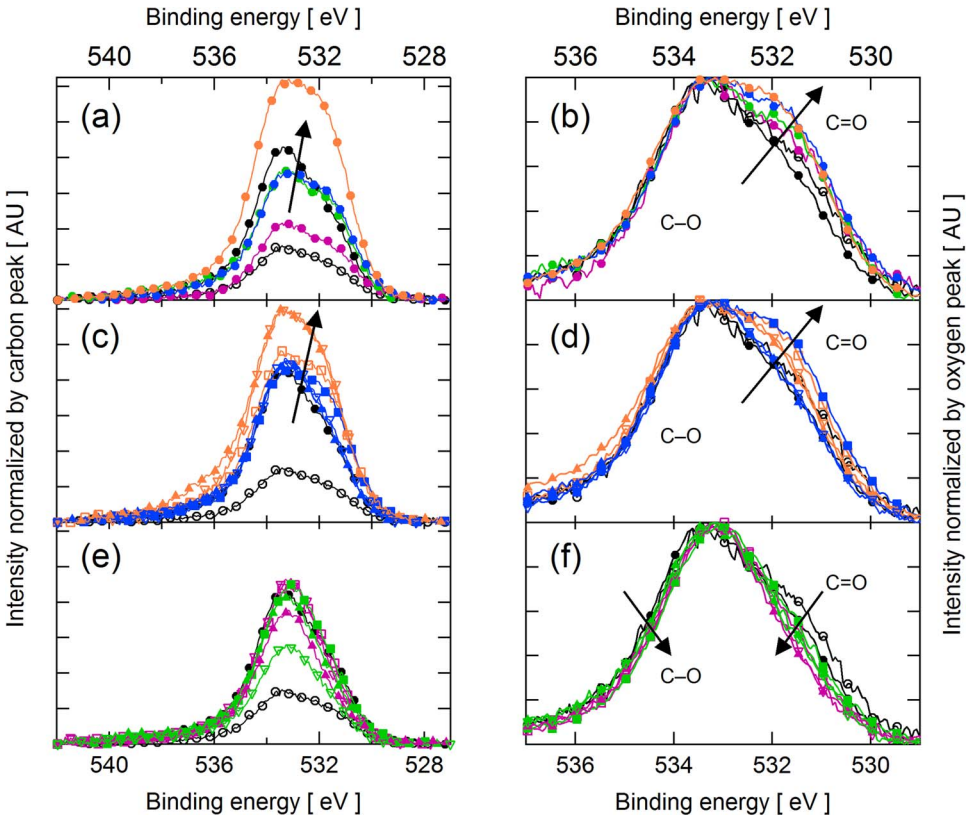

Figure 7. XPS O1s spectra for electrodes subjected to soaking and cell-in-series operation for 3 d: (a) soaked electrodes normalized by C1s peak, (b) soaked electrodes normalized by O1s peak, (c) positive electrodes normalized by C1s peak, (d) positive electrodes normalized by O1s peak, (e) negative electrodes normalized by C1s peak, and (f) negative electrodes normalized by O1s peak. Pristine (○) and acid soaked (●) included for reference in all frames. Color scheme refers to electrode polarity and SoC as follows: (●) + high SoC, (●) + low SoC, (●) – low SoC, (●) – high SoC. Symbol shape refers to experimental condition as follows: (●) soaked, (▽) −20 mA/cm^2, (▲) +20 mA/cm^2, (■) +200 mA/cm^2, (□) −200 mA/cm^2. (a), (c), and (e) are plotted on identical vertical axes.

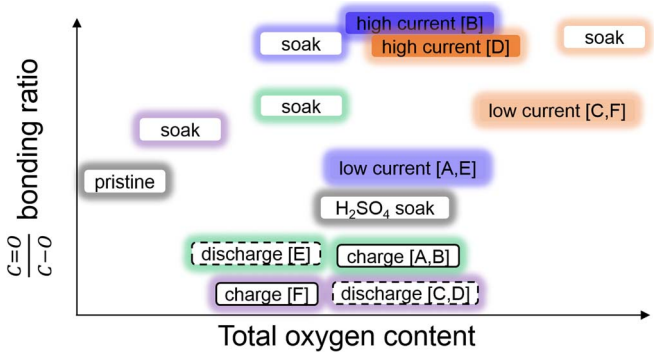

Figure 8. Qualitative comparison of oxygen content and bonding for electrodes analyzed with XPS.

that carbon paper and carbon felts likely exhibit different operational lifetimes under continued electrochemical stress.

The surface chemistry of the carbon electrode was affected by soaking in the vanadium electrolyte as well as during VRFB operation. However, the electrode performance was only affected by VRFB operation. Because drastically different electrode overpotentials were observed for electrodes with similar oxygen content, the results seem to indicate that the oxygen content of the electrode surface does not play a major role in decreasing the electrochemical performance of the carbon materials tested. Melke et al.[47] found that heat-treated carbon materials do not rely upon carboxyl or hydroxyl groups to facilitate the vanadium redox reactions. Combined, these results suggest that oxygen groups may not play a significant role in the vanadium redox reactions. These findings contrast with the theory advanced in references 14 and 20 that the loss of oxygen functional groups on the anode contributes to increased cell polarization. Thus, more work is required to determine the cause(s) of electrode performance loss, as the surface area and oxygen-related surface chemistry were found to be unlikely causes for the changes observed in electrode performance in this work. It is noted that degradation mechanisms may differ for felt vs. paper-based electrodes.

Conclusions

In this work, we show the origin of changes in the energy efficiency that occurred in a typical cycling experiment. The combined activation and concentration polarization increased from 25 mV pre-cycling to 45 mV after 54 cycles at 200 mA/cm^2; ohmic overpotential, presumably due to membrane fouling, increased 20 mV. These increases in overpotential together contributed 22% to the observed capacity fade after 54 cycles, while crossover accounted for 12%. The CIS set-up was then introduced as a method to study constant conditions in flow battery testing, and reasonably constant conditions were achieved. We demonstrate that charging at high SoC and discharging at low SoC can be used to accelerate performance loss in VRFBs, and that the CIS design can therefore assist in material durability evaluation. Analysis of the polarization curves suggests that both the charging and discharging process contribute to decreased electrode performance; therefore, neither process is solely responsible for performance loss. Simple exposure to electrolyte with no electrochemical cycling had no significant effect on the kinetic performance of the electrode.

Electrode samples from CIS experiments and from electrolyte soaks were analyzed with XPS to determine changes in the surface chemistry. High SoC induced the most oxidation on the positive electrode, with oxygen content of up to 9.3%; the negative electrode exhibited oxidation similar to that caused by soaking in sulfuric acid, around 5.5%. Changes in the C–O/C=O chemistry were primarily related to the polarity of the battery and were more sensitive to operating conditions on the positive electrode. XPS results in conjunction with polarization curve analysis suggest that the oxygen content on its own may not play a large role in electrode performance for the electrode materials tested, and therefore that aging-related changes in oxygen cannot explain the observed electrode performance loss.

The CIS technique, which allows for constant condition testing, provides a platform for these insights into how SoC, magnitude of current, and direction of current affect degradation mechanisms in VRFBs. The use of XPS to examine oxygen content is a demonstration of how the CIS can be used in conjunction with an analytic technique to study targeted physicochemical properties of the electrode as a function of SoC and applied current. The study of electrodes after cycling does not allow the freedom to distinguish which portion of the charge/discharge cycle (i.e., at which SoC, charge or discharge) might contribute to changes in the material properties, which is where the CIS can be of great benefit. This work rules out changes in oxygen functionality and surface area as likely causes of the loss in electrode performance. More work must be done to better understand how other physicochemical properties change during battery operation, and which properties are important to declining performance.

While the CIS technique is used in this work to study the effect of a constant condition on the electrode in VRFBs, it should be noted that the technique could be applied to other flow battery chemistries and experiments. The CIS can be used to study membrane durability in a manner similar to how electrodes were studied in this work. Membrane permeability measurements could also be taken at constant SoC from an operating battery. The CIS can also provide a useful platform for other types of flow battery experiments. Short-term experiments that would benefit from a constant SoC, including polarization curve analysis, could utilize a counter-cell to maintain SoC, as opposed to a single-pass configuration which requires a large volume of electrolyte or low flow rates in order to conduct a constant SoC experiment. Symmetric cells[48] are another useful tool to conduct constant SoC experiments; one may find the CIS technique advantageous because SoC can be changed by changing conditions in the counter-cell, whereas a symmetric cell requires changing of the electrolyte solution to change SoC.

Acknowledgments

Funding for experimental work was provided by the Office of Naval Research work under Long Range Broad Agency Announcement (BAA) #N00014-12-1-0887. A portion of this work (GMV-XPS) was supported by U.S. Department of Energy's Office of Basic Energy Science (DOE-BES), Division of Materials Sciences and Engineering, under contract with UT-Battelle, LLC. Additional personnel support for experiments (RLS) was provided by the Fluid Interface Reactions Structures and Transport (FIRST) Center, an Energy Frontier Research Center funded by the U.S. Department of Energy, Officer of Science, Office of Basic Sciences. The authors thank Drs. E.L. Redmond and D.S. Aaron for fruitful discussion.

References

1. Z. Yang, J. Zhang, M. C. W. Kintner-Meyer, X. Lu, D. Choi, J. P. Lemmon, and J. Liu, *Chem. Rev.*, **111**, 3577 (2011).
2. A. Z. Weber, M. M. Mench, J. P. Meyers, P. N. Ross, J. T. Gostick, and Q. Liu, *J. Appl. Electrochem.*, **41**, 1137 (2011).
3. A. Parasuraman, T. M. Lim, C. Menictas, and M. Skyllas-Kazacos, *Electrochim. Acta*, **101**, 27 (2013).
4. M. Skyllas-Kazacos, M. H. Chakrabarti, S. A. Hajimolana, F. S. Mjalli, and M. Saleem, *J. Electrochem. Soc.*, **158**, R55 (2011).
5. P. Leung, X. Li, C. Ponce de León, L. Berlouis, C. T. J. Low, and F. C. Walsh, *RSC Adv.*, **2**, 10125 (2012).
6. D. S. Aaron, Q. Liu, Z. Tang, G. M. Grim, A. B. Papandrew, A. Turhan, T. A. Zawodzinski, and M. M. Mench, *J. Power Sources*, **206**, 450 (2012).
7. Q. H. Liu, G. M. Grim, A. B. Papandrew, A. Turhan, T. A. Zawodzinski, and M. M. Mench, *J. Electrochem. Soc.*, **159**, A1246 (2012).
8. X. Li, H. Zhang, Z. Mai, H. Zhang, and I. Vankelecom, *Energy Environ. Sci.*, **4**, 1147 (2011).
9. C.-N. Sun, Z. Tang, C. Belcher, T. A. Zawodzinski, and C. Fujimoto, *Electrochem. Commun.*, **43**, 63 (2014).
10. A. M. Pezeshki, J. T. Clement, G. M. Veith, T. A. Zawodzinski, and M. M. Mench, *J. Power Sources*, **294**, 333 (2015).
11. J. Zhang, L. Li, Z. Nie, B. Chen, M. Vijayakumar, S. Kim, W. Wang, B. Schwenzer, J. Liu, and Z. Yang, *J. Appl. Electrochem.*, **41**, 1215 (2011).

12. H. Han, Z. He, J. Liu, Y. Chen, and S. Liu, *Ionics*, **21**, 167 (2015).
13. L. Li, S. Kim, W. Wang, M. Vijayakumar, Z. Nie, B. Chen, J. Zhang, G. Xia, J. Hu, G. Graff, J. Liu, and Z. Yang, *Adv. Energy Mater.*, **1**, 394 (2011).
14. S. Rudolph, U. Schröder, and I. M. Bayanov, *J. Electroanal. Chem.*, **703**, 29 (2013).
15. M. Skyllas-Kazacos and M. Kazacos, *J. Power Sources*, **196**, 8822 (2011).
16. S. Corcuera and M. Skyllas-Kazacos, *Eur. Chem. Bull.*, **1**, 511 (2012).
17. M. Rychcik and M. Skyllas-Kazacos, *J. Power Sources*, **22**, 59 (1988).
18. P. Trogadas, O. O. Taiwo, B. Tjaden, T. P. Neville, S. Yun, J. Parrondo, V. Ramani, M.-O. Coppens, D. J. L. Brett, and P. R. Shearing, *Electrochem. Commun.*, **48**, 155 (2014).
19. F. Mohammadi, P. Timbrell, S. Zhong, C. Padeste, and M. Skyllas-Kazacos, *J. Power Sources*, **52**, 61 (1994).
20. S. Rudolph, U. Schröder, I. M. Bayanov, and D. Hage, *J. Electroanal. Chem.*, **728**, 72 (2014).
21. S. Rudolph, U. Schröder, I. M. Bayanov, and G. Pfeiffer, *J. Electroanal. Chem.*, **709**, 93 (2013).
22. H. Liu, Q. Xu, and C. Yan, *Electrochem. Commun.*, **28**, 58 (2013).
23. H. Liu, Q. Xu, C. Yan, and Y. Qiao, *Electrochim. Acta*, **56**, 8783 (2011).
24. A. J. Bard and L. R. Faulkner, *Electrochemical Methods: Fundamentals and Applications*, Second, John Wiley & Sons, Inc., Hoboken, NJ (2001).
25. J. Newman and K. E. Thomas-Alyea, *Electrochemical Systems*, Third, John Wiley & Sons, Inc., Hoboken, NJ (2004).
26. B. Sun and M. Skyllas-Kazacos, *Electrochim. Acta*, **37**, 1253 (1992).
27. B. Sun and M. Skyllas-Kazacos, *Electrochim. Acta*, **37**, 2459 (1992).
28. T. Wu, K. Huang, S. Liu, S. Zhuang, D. Fang, S. Li, D. Lu, and A. Su, *J. Solid State Electrochem.*, **16**, 579 (2011).
29. C. Flox, M. Skoumal, J. Rubio-Garcia, T. Andreu, and J. R. Morante, *Appl. Energy*, **109**, 344 (2013).
30. C. Gao, N. Wang, S. Peng, S. Liu, Y. Lei, X. Liang, S. Zeng, and H. Zi, *Electrochim. Acta*, **88**, 193 (2013).
31. Z. González, C. Botas, P. Álvarez, S. Roldán, C. Blanco, R. Santamaría, M. Granda, and R. Menéndez, *Carbon*, **50**, 828 (2012).
32. P. Han, Y. Yue, Z. Liu, W. Xu, L. Zhang, H. Xu, S. Dong, and G. Cui, *Energy Environ. Sci.*, **4**, 4710 (2011).
33. P. Han, H. Wang, Z. Liu, X. Chen, W. Ma, J. Yao, Y. Zhu, and G. Cui, *Carbon*, **49**, 693 (2011).
34. K. J. Kim, Y.-J. Kim, J.-H. Kim, and M.-S. Park, *Mater. Chem. Phys.*, **131**, 547 (2011).
35. W. Li, J. Liu, and C. Yan, *Electrochim. Acta*, **79**, 102 (2012).
36. Y. Shao, X. Wang, M. Engelhard, C. Wang, S. Dai, J. Liu, Z. Yang, and Y. Lin, *J. Power Sources*, **195**, 4375 (2010).
37. S. Wang, X. Zhao, T. Cochell, and A. Manthiram, *J. Phys. Chem. Lett.*, **3**, 2164 (2012).
38. L. Yue, W. Li, F. Sun, L. Zhao, and L. Xing, *Carbon*, **48**, 3079 (2010).
39. A. Di Blasi, O. Di Blasi, N. Briguglio, A. S. Aricò, D. Sebastián, M. J. Lázaro, G. Monforte, and V. Antonucci, *J. Power Sources*, **227**, 15 (2013).
40. M. M. Mench, *Fuel Cell Engines*, John Wiley & Sons, Inc., Hoboken, NJ (2008).
41. M. Vijayakumar, M. S. Bhuvaneswari, P. Nachimuthu, B. Schwenzer, S. Kim, Z. Yang, J. Liu, G. L. Graff, S. Thevuthasan, and J. Hu, *J. Membr. Sci.*, **366**, 325 (2011).
42. R. M. Darling, A. Z. Weber, M. C. Tucker, and M. L. Perry, *J Electrochem. Soc.*, **163**, A5014 (2016).
43. D. Chen and M. A. Hickner, *Phys. Chem. Chem. Phys.*, **15**, 11299 (2013).
44. C.-T. Hsieh and H. Teng, *Carbon*, **40**, 667 (2002).
45. C.-N. Sun, F. M. Delnick, L. Baggetto, G. M. Veith, and T. A. Zawodzinski, *J. Power Sources*, **248**, 560 (2014).
46. G. J. Brug, A. L. G. van den Eeden, M. Sluyters-Rehbach, and J. H. Sluyters, *J. Electroanal. Chem. Interfacial Electrochem.*, **176**, 275 (1984).
47. J. Melke, P. Jakes, J. Langner, L. Riekehr, U. Kunz, Z. Zhao-Karger, A. Nefedov, H. Sezen, C. Wöll, H. Ehrenberg, and C. Roth, *Carbon*, **78**, 220 (2014).
48. R. M. Darling and M. L. Perry, *ECS Trans.*, **53**, 31 (2013).